Downloaded from http://rspa.royalsocietypublishing.org/ on December 5, 2016

PROCEEDINGS A

rspa.royalsocietypublishing.org

Research

Cite this article: Yuan J, Dagdeviren C, Shi Y, Ma Y, Feng X, Rogers JA, Huang Y. 2016 Computational models for the determination of depth-dependent mechanical properties of skin with a soft, flexible measurement device. *Proc. R. Soc. A* **472**: 20160225.
http://dx.doi.org/10.1098/rspa.2016.0225

Received: 30 March 2016
Accepted: 16 September 2016

Subject Areas:
mechanical engineering, mechanics

Keywords:
conformal modulus sensors, skin moduli, epidermis and dermis, electromechanical coupling

Authors for correspondence:
John A. Rogers
e-mail: jrogers@illinois.edu
Yonggang Huang
e-mail: y-huang@northwestern.edu

Computational models for the determination of depth-dependent mechanical properties of skin with a soft, flexible measurement device

Jianghong Yuan[1,2,3,4,5,6,†], Canan Dagdeviren[7,8,†], Yan Shi[1,2], Yinji Ma[1,2,3,4,5,6], Xue Feng[1,2], John A. Rogers[9,10] and Yonggang Huang[3,4,5,6]

[1]Center for Mechanics and Materials and [2]AML, Department of Engineering Mechanics, Tsinghua University, Beijing 100084, People's Republic of China
[3]Department of Civil an Environmental Engineering, [4]Department of Mechanical Engineering, [5]Department of Materials Science and Engineering and [6]Skin Disease Research Center, Northwestern University, Evanston, IL 60208, USA
[7]The David H. Koch Institute for Integrative Cancer Research, Massachusetts Institute of Technology, Cambridge, MA 02139, USA
[8]Harvard Society of Fellows, Harvard University, Cambridge, MA 02138, USA
[9]Department of Materials Science and Engineering, and [10]Frederick Seitz Materials Research Laboratory, University of Illinois at Urbana-Champaign, Urbana, IL 61801, USA

YH, 0000-0002-0483-8359

Conformal modulus sensors (CMS) incorporate PZT nanoribbons as mechanical actuators and sensors to achieve reversible conformal contact with the human skin for non-invasive, *in vivo* measurements of skin modulus. An analytic model presented in this paper yields expressions that connect the sensor output voltage to the Young moduli of the epidermis and dermis, the thickness of the epidermis, as well as the material and geometrical parameters of the CMS device itself and its encapsulation layer. Results from the model agree well with *in vitro* experiments on bilayer structures of poly(dimethylsiloxane).

[†]These authors contributed equally to the study.

THE ROYAL SOCIETY PUBLISHING

© 2016 The Author(s) Published by the Royal Society. All rights reserved.

Downloaded from http://rspa.royalsocietypublishing.org/ on December 5, 2016

These results provide a means to determine the skin moduli (epidermis and dermis) and the thickness of the epidermis from *in vivo* measurements of human skin.

1. Introduction

Human skin is a complex living tissue consisting of several heterogeneous layers, namely the epidermis (composed of the stratum corneum and the viable epidermis) [1], the dermis (composed of the superficial papillar dermis and the collagen-rich reticular dermis) [2] and the hypodermis (i.e. the subcutaneous fat) overlying the subcutaneous tissue (i.e. the muscle) [3]. Although the human skin behaves as nonlinear, viscoelastic, anisotropic, inhomogeneous and incompressible material [4], the effective Young's modulus remains a key parameter that characterizes its overall mechanical properties [5,6]. Determination of the Young modulus of each component layer of the human skin is of critical importance for cosmetic and clinical applications, of relevance in the efficacy of cosmetic products such as creams [7], drug delivery using microneedles or microjets [1], and diagnosis of various skin diseases such as scleroderma, Ehlers–Danlos and skin cancer [6,8].

For measuring the Young modulus of human skin, various experimental methods have been developed, e.g. indentation [1,3], suction [2,4,7], torsion [5,9], traction [10,11], elastography [6] and surface wave propagation [12]. By performing *in vivo* suction experiments with different aperture diameters, Hendriks *et al.* [2] found a large difference in stiffness between the reticular dermis layer and the upper layer consisting of the epidermis and the papillar dermis. The results verified, to a certain extend, the hypothesis that experiments with different length scales can capture the mechanical behaviour of different layers of human skin. By using a spherical tip with a large diameter compared with the sample thickness in *in vitro* microindentation experiments, Geerligs *et al.* [1] observed no significant differences in stiffness between the stratum corneum and the viable epidermis of human skin. From *in vivo* indentation experiments using a conical steel indenter with a height of 10 mm, Pailler-Mattei *et al.* [3] concluded that it is necessary to take into account the effect of the subcutaneous fat and muscle to estimate the Young modulus of human skin correctly. Hendriks *et al.* [4] showed, however, that contribution from the subcutaneous fat layer to the mechanical response of the human skin is negligible in suction experiments, using an aperture size of 6 mm. By measuring the surface waves induced by short impulses via the phase-sensitive optical coherence tomography, Li *et al.* [12] successfully evaluated the Young moduli of the dermis and the subcutaneous fat of human skin. These experiments did not, however, yield the Young moduli of the thin epidermis, because the excitation frequency and the sampling frequency they used in *in vivo* experiments were not sufficiently high.

In recent years, stretchable and flexible electronics have emerged in forms that allow accurate measurements of electrophysiological signals and thermal and mechanical properties of the human body [13–23]. Dagdeviren *et al.* [24] reported a microconformal modulus sensor (CMS) system that can achieve soft and reversible conformal contact with the underlying complex topography and texture of the human skin, and surfaces of other organs of the body, to provide accurate and reproducible non-invasive measurements of the modulus. In this paper, we develop an analytical model to extend Dagdeviren *et al.*'s experimental design [24] to simultaneous determination of the Young moduli of the epidermis and dermis layers as well as the epidermis thickness. The paper is organized as follows. The geometrical and material properties of the proposed model are described in detail in §2. The analytic model, which accounts for the interaction between the CMS system and the multi-layered skin, is discussed in detail in §3. The analytic model is then compared with a validation experiment. Section 4 presents a strategy to extract the skin moduli (epidermis and dermis) and the epidermis thickness from data obtained from the CMS system. The paper concludes with some summary remarks in §5. We emphasize here that this is mostly an analytical paper, rather than an experimental paper, with figures 3–6 being the main analytical results of our theoretical model.

Downloaded from http://rspa.royalsocietypublishing.org/ on December 5, 2016

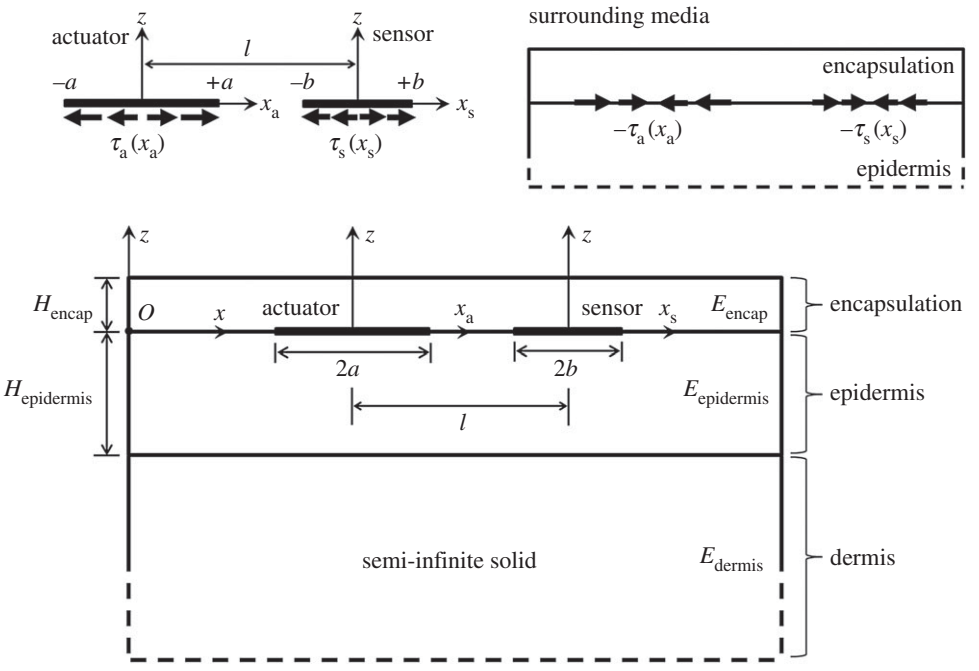

Figure 1. Bilayered structure of the human skin and conformal modulus sensor (CMS) system mounted on the surface with encapsulation, where (x_a, z) and (x_s, z) are the local coordinates with the origin at the centres of the actuator and sensor, respectively; (x, z) is the global coordinates. The actuator, the sensor and the surrounding media interact through the resultant, distributed shear forces τ_a and τ_s at their interfaces.

2. Model description

As shown in figure 1, by neglecting the extremely soft subcutaneous fat [4], the human skin can be approximately modelled as a bilayered system: an elastic epidermis layer with the thickness $H_{epidermis}$ and Young modulus $E_{epidermis}$ and an elastic dermis layer with the Young modulus E_{dermis}. The dermis layer is much thicker (e.g. approx. 1 mm [12,25]) than the epidermis (e.g. approx. 0.1 mm [12,25]) and is therefore simplified as a semi-infinite solid. Their Poisson's ratios are 0.5 because of the incompressibility.

A CMS system with an encapsulation layer (thickness H_{encap}, Young's modulus E_{encap}, and Poisson's ratio 0.5) is mounted on the surface of the human skin (figure 1). The piezoelectric actuator (length $2a$) and sensor (length $2b$) in the CMS system are laminates composed of seven parallel layers with a total thickness of about 5 µm [24]. The fourth (middle) layer among them is made of PZT-4 with a thickness of h_{PZT} (≈0.5 µm [24]), and the poling direction of PZT-4 is along its thickness. The geometrical and material properties of each constituent layer are listed in appendix A. The spacing between the centres of a pair of sensors and actuators is l.

The model is two-dimensional with plane-strain deformation. The inertia effect is negligible owing to the low working frequency (below 1000 Hz) of the CMS system [24] such that the harmonic vibrations in the experiments can be treated as a quasi-static problem.

The piezoelectric actuator is subjected to an input voltage U_{input}. Under the applied electric field E_z along the poling direction of the PZT-4 layer, the actuator expands in the thickness direction, and shrinks in the length direction owing to the inverse piezoelectric effect. Because the length (approx. 10^2 µm [24]) of the actuator (or sensor) is much larger than its thickness (≈5 µm [24]), the length-shrinking mode dominates the deformation. The actuator (or sensor) can then be modelled as an electro-elastic line with zero thickness [26] to impose a resultant shear force distribution onto the surrounding media along the interface between the encapsulation layer

Downloaded from http://rspa.royalsocietypublishing.org/ on December 5, 2016

and the epidermis layer at the location of the actuator (figure 1). The shear force deforms the surrounding media and then lengthens the piezoelectric sensor in its length direction, which results in an output voltage from the sensor owing to the direct piezoelectric effect under the open-loop electrical boundary condition.

The analytical solution in §3 gives the relation between the output voltage of the sensor and the input voltage of the actuator in terms of the Young moduli of the epidermis and dermis layers and the thickness of the epidermis layer, which forms the basis for measuring the skin modulus.

3. Analytical solution

It should be pointed out that the bending mode also exists during deformations of the laminated actuator/sensor, but it makes little contribution to the axial strain of the PZT-4 layer, because the neutral axis of bending of the actuator/sensor is inside the PZT-4 layer. The bending effect of the actuator/sensor on the output voltage of the sensor is therefore neglected.

(a) Analysis of the actuator and the sensor

As shown in figure 1, let (x_a, z) and (x_s, z) be the local coordinates with the origin at the centres of the actuator and sensor, respectively, with the z-axis normal to the interface and x-axis direction from the actuator to the sensor (figure 1). The resultant, distributed shear force on the actuator and the sensor, is denoted by $\tau_a(x_a)$ and $\tau_s(x_s)$, respectively. Force equilibrium of the actuator and the sensor requires

$$\int_{-a}^{a} \tau_a(\xi_a)\,\mathrm{d}\xi_a = 0 \quad \text{and} \quad \int_{-b}^{b} \tau_s(\xi_s)\,\mathrm{d}\xi_s = 0, \tag{3.1}$$

which results from the traction-free condition at both ends of the actuator or the sensor, because (i) the thickness of the actuator/sensor is extremely small ($\approx$5 µm [24]) as compared with its length (approx. 10^2 µm [24]) and (ii) the Young moduli (approx. 10^2 kPa [24]) of the surrounding encapsulation and epidermis are many orders of magnitude smaller than that of the actuator/sensor (approx. 10^2 GPa [24]).

The equilibrium equations are

$$\frac{\partial}{\partial x_a}\sum_{k=1}^{7}\sigma_a^{(k)}(x_a)h^{(k)} + \tau_a(x_a) = 0 \quad \text{and} \quad \frac{\partial}{\partial x_s}\sum_{k=1}^{7}\sigma_s^{(k)}(x_s)h^{(k)} + \tau_s(x_s) = 0, \tag{3.2}$$

where the superscript k means the kth layer of the laminated actuator/sensor; $h^{(k)}$, $\sigma_a^{(k)}$ and $\sigma_s^{(k)}$ denote the thickness and the axial stress of the kth layer of the actuator or the sensor, respectively. Integration of equation (3.2) gives

$$\sum_{k=1}^{7}\sigma_a^{(k)}(x_a)h^{(k)} = -\int_{-a}^{x_a}\tau_a(\xi_a)\,\mathrm{d}\xi_a \quad \text{and} \quad \sum_{k=1}^{7}\sigma_s^{(k)}(x_s)h^{(k)} = -\int_{-b}^{x_s}\tau_s(\xi_s)\,\mathrm{d}\xi_s. \tag{3.3}$$

The axial strain of actuator and sensor, which should be the same in all constituent layers and be continuous across their interfaces with the surrounding media, is denoted by ε_a and ε_s. The constitutive relations for each constituent layer of the actuator and the sensor are [26,27]

$$\sigma_a^{(k)} = \begin{cases} \bar{E}_a^{(4)}\varepsilon_a - e_p E_z, & (k=4) \\ \bar{E}_a^{(k)}\varepsilon_a, & \text{otherwise} \end{cases} \quad \text{and} \quad \sigma_s^{(k)} = \bar{E}_s^{(k)}\varepsilon_s, (k=1,2,\ldots,7), \tag{3.4}$$

Downloaded from http://rspa.royalsocietypublishing.org/ on December 5, 2016

with E_z being the electric field in the PZT layer of the actuator and

$$\left.\begin{aligned}\bar{E}_{\mathrm{a}}^{(k)} &= \begin{cases} c_{11} - \dfrac{c_{13}^2}{c_{33}}, & k=4 \\ \dfrac{E^{(k)}}{1-(\nu^{(k)})^2}, & \text{otherwise} \end{cases}; \quad \bar{E}_{\mathrm{s}}^{(k)} = \begin{cases} c_{11} - \dfrac{c_{13}^2}{c_{33}} + \dfrac{e_{\mathrm{p}}^2}{k_{\mathrm{e}}}, & k=4 \\ \dfrac{E^{(k)}}{1-(\nu^{(k)})^2}, & \text{otherwise} \end{cases}; \\ e_{\mathrm{p}} &= e_{31} - e_{33}\frac{c_{13}}{c_{33}}; \quad k_{\mathrm{e}} = k_{33} + \frac{e_{33}^2}{c_{33}} \end{aligned}\right\}, \tag{3.5}$$

where c_{ij}, e_{ij} and k_{ij} are the elastic, piezoelectric and dielectric constants of PZT-4, respectively; $E^{(k)}$ is the Young modulus and $\nu^{(k)}$ is the Poisson's ratio of the kth layer.

Substitution of equation (3.4) into equation (3.3) gives the axial strains of the actuator and the sensor as

$$\varepsilon_{\mathrm{a}}(x_{\mathrm{a}}) = -\frac{1}{K_{\mathrm{a}}}\int_{-a}^{x_{\mathrm{a}}} \tau_{\mathrm{a}}(\xi_{\mathrm{a}})\,\mathrm{d}\xi_{\mathrm{a}} + \frac{e_{\mathrm{p}}h_{\mathrm{PZT}}}{K_{\mathrm{a}}}E_z \quad \text{and} \quad \varepsilon_{\mathrm{s}}(x_{\mathrm{s}}) = -\frac{1}{K_{\mathrm{s}}}\int_{-b}^{x_{\mathrm{s}}} \tau_{\mathrm{s}}(\xi_{\mathrm{s}})\,\mathrm{d}\xi_{\mathrm{s}}, \tag{3.6}$$

with

$$K_{\mathrm{a}} = \sum_{k=1}^{7} \bar{E}_{\mathrm{a}}^{(k)} h^{(k)} \quad \text{and} \quad K_{\mathrm{s}} = \sum_{k=1}^{7} \bar{E}_{\mathrm{s}}^{(k)} h^{(k)}. \tag{3.7}$$

The second relation of equation (3.6), together with vanishing electric displacement $D_z(x_{\mathrm{s}}) = e_{\mathrm{p}}\varepsilon_{\mathrm{s}}(x_{\mathrm{s}}) + k_{\mathrm{e}}E'_z(x_{\mathrm{s}}) = 0$ [27] in the PZT-4 layer of the sensor, gives the ratio of the output voltage of the sensor to the input voltage of the actuator as [27]

$$\frac{U_{\mathrm{output}}}{U_{\mathrm{input}}} = \frac{(1/2b)\int_{-b}^{b}[-E'_z(x_{\mathrm{s}})h_{\mathrm{PZT}}]\,\mathrm{d}x_{\mathrm{s}}}{-E_z h_{\mathrm{PZT}}} = \frac{e_{\mathrm{p}}}{k_{\mathrm{e}}K_{\mathrm{s}}E_z}\frac{1}{2b}\int_{-b}^{b}\mathrm{d}x_{\mathrm{s}}\int_{-b}^{x_{\mathrm{s}}}\tau_{\mathrm{s}}(\xi_{\mathrm{s}})\,\mathrm{d}\xi_{\mathrm{s}}, \tag{3.8}$$

where $E'_z(x_{\mathrm{s}})$ is the distributed electric field in the PZT-4 layer (sandwiched by two electrodes) of the sensor.

(b) Analysis of the surrounding media

Let $\varepsilon(x;\xi)$ denote the normal strain in the x-direction (figure 1) at point $(x, 0)$ (i.e. the interface between the encapsulation and the epidermis) owing to a concentrated force of unit magnitude along the positive x-axis (figure 1) applied at point $(\xi, 0)$. It can be decomposed into two separate parts as follows (see appendix B)

$$\varepsilon(x;\xi) = \varepsilon_{\mathrm{epidermis}}^{\mathrm{encap}}(x;\xi) + \varepsilon_{\mathrm{dermis}}^{\mathrm{free\text{-}surface}}(x;\xi), \tag{3.9}$$

where the first term on its right-hand side denotes the normal strain owing to the same force in the corresponding bimaterial composed of an encapsulation half-plane and an epidermis half-plane; and the second term accounts for the effects of both the free-surface of the encapsulation layer and the semi-infinite dermis. Generalization of the method of reverberation ray matrix [28–30] from elastodynamics to elastostatics gives these two terms as (see appendix B for details)

$$\varepsilon_{\mathrm{epidermis}}^{\mathrm{encap}}(x;\xi) = -\frac{3}{2\pi(E_{\mathrm{encap}} + E_{\mathrm{epidermis}})}\frac{1}{x-\xi} \tag{3.10}$$

and

$$\varepsilon_{\mathrm{dermis}}^{\mathrm{free\text{-}surface}}(x;\xi) = -\frac{3}{2\pi(E_{\mathrm{encap}} + E_{\mathrm{epidermis}})}\int_0^{+\infty} f(k)\sin[k(x-\xi)]\,\mathrm{d}k, \tag{3.11}$$

with

$$f(k) = \mathbf{c}^{\mathrm{T}}(k)\,\mathbf{d}(k). \tag{3.12}$$

Downloaded from http://rspa.royalsocietypublishing.org/ on December 5, 2016

Here,

$$\left.\begin{aligned}\mathbf{c}(k) &= [\mathbf{c}_{\text{encap}}(k) \quad \mathbf{0}_{1\times4} \quad \mathbf{0}_{1\times2}]^{\mathrm{T}} \\ \text{and} \qquad \mathbf{c}_{\text{encap}}(k) &= [\mathrm{e}^{-kH_{\text{encap}}} \quad H_{\text{encap}}\,\mathrm{e}^{-kH_{\text{encap}}} \quad 1 \quad 0]\end{aligned}\right\} \tag{3.13}$$

and

$$\mathbf{d}(k) = [\mathbf{I}_{10\times10} + \mathbf{S}(k)\mathbf{P}(k)]^{-1}\mathbf{s}(k) - \mathbf{s}(k), \tag{3.14}$$

where 'T' denotes the transpose of a matrix or a vector, '**I**' denotes the identity matrix and the scattering matrix $\mathbf{S}(k)$ is defined only in terms of material parameters as

$$\mathbf{S}(k) = \begin{bmatrix} \mathbf{S}^{\text{free-surface}}(k) & \mathbf{0}_{2\times4} & \mathbf{0}_{2\times2} \\ \mathbf{0}_{4\times2} & \mathbf{S}(k;\alpha^{\text{encap}}_{\text{epidermis}}) & \mathbf{0}_{4\times2} \\ \mathbf{0}_{4\times2} & \mathbf{0}_{4\times4} & \mathbf{S}^{\text{half-space}}(k;\alpha^{\text{epidermis}}_{\text{dermis}}) \end{bmatrix}, \tag{3.15}$$

with

$$\left.\begin{aligned}\mathbf{S}(k;\alpha) &= \begin{bmatrix} -\alpha & 0 & -1+\alpha & 0 \\ 2\alpha k & -\alpha & 0 & 1-\alpha \\ -1-\alpha & 0 & \alpha & 0 \\ 0 & 1+\alpha & -2\alpha k & \alpha \end{bmatrix} \\ \mathbf{S}^{\text{half-space}}(k;\alpha) &= \begin{bmatrix} -\alpha & 0 \\ 2\alpha k & -\alpha \\ -1-\alpha & 0 \\ 0 & 1+\alpha \end{bmatrix} \\ \text{and} \qquad \mathbf{S}^{\text{free-surface}}(k) &= \begin{bmatrix} -1 & 0 \\ 2k & -1 \end{bmatrix}\end{aligned}\right\}, \tag{3.16}$$

where

$$\alpha^{\text{encap}}_{\text{epidermis}} = \frac{E_{\text{encap}} - E_{\text{epidermis}}}{E_{\text{encap}} + E_{\text{epidermis}}} \quad \text{and} \quad \alpha^{\text{epidermis}}_{\text{dermis}} = \frac{E_{\text{epidermis}} - E_{\text{dermis}}}{E_{\text{epidermis}} + E_{\text{dermis}}}, \tag{3.17}$$

are the first Dundurs' parameter [31] for the encapsulation/epidermis and epidermis/dermis interfaces, respectively. The phase matrix $\mathbf{P}(k)$ in equation (3.14) is defined only in terms of geometric parameters as

$$\mathbf{P}(k) = \begin{bmatrix} \mathbf{P}(k;H_{\text{encap}}) & \mathbf{0}_{4\times4} & \mathbf{0}_{4\times2} \\ \mathbf{0}_{4\times4} & \mathbf{P}(k;H_{\text{epidermis}}) & \mathbf{0}_{4\times2} \end{bmatrix}, \tag{3.18}$$

with

$$\mathbf{P}(k;H) = \begin{bmatrix} 0 & 0 & e^{-kH} & He^{-kH} \\ 0 & 0 & 0 & -e^{-kH} \\ e^{-kH} & He^{-kH} & 0 & 0 \\ 0 & -e^{-kH} & 0 & 0 \end{bmatrix}. \tag{3.19}$$

The source vector $\mathbf{s}(k)$ in equation (3.14) is defined as

$$\left.\begin{aligned}\mathbf{s}(k) &= [\mathbf{0}_{1\times2} \quad \mathbf{s}^{\text{encap}}_{\text{epidermis}}(k) \quad \mathbf{0}_{1\times4}]^{\mathrm{T}} \\ \text{and} \qquad \mathbf{s}^{\text{encap}}_{\text{epidermis}}(k) &= [1 \quad -k \quad 1 \quad -k]\end{aligned}\right\}. \tag{3.20}$$

The normal strains in the x-direction (figure 1) of surrounding media along the encapsulation–epidermis interface at the locations of the actuator and the sensor are denoted by $\varepsilon_{\text{i-a}}$ and $\varepsilon_{\text{i-s}}$, respectively, and are obtained via the principle of superposition as

$$\left.\begin{aligned}\varepsilon_{\text{i-a}}(x_{\text{a}}) &= -\int_{-a}^{a} \tau_{\text{a}}(\xi_{\text{a}})\varepsilon(x_{\text{a}};\xi_{\text{a}})\,\mathrm{d}\xi_{\text{a}} - \int_{-b}^{b} \tau_{\text{s}}(\xi_{\text{s}})\varepsilon(x_{\text{a}};\xi_{\text{s}}+l)\,\mathrm{d}\xi_{\text{s}} \\ \text{and} \qquad \varepsilon_{\text{i-s}}(x_{\text{s}}) &= -\int_{-a}^{a} \tau_{\text{a}}\,(\xi_{\text{a}})\,\varepsilon\,(x_{\text{s}};\xi_{\text{a}}-l)\,\mathrm{d}\xi_{\text{a}} - \int_{-b}^{b} \tau_{\text{s}}(\xi_{\text{s}})\varepsilon(x_{\text{s}};\xi_{\text{s}})\,\mathrm{d}\xi_{\text{s}}\end{aligned}\right\}. \tag{3.21}$$

Downloaded from http://rspa.royalsocietypublishing.org/ on December 5, 2016

(c) Interactions among the actuator, sensor and surrounding media

The continuity of axial strains requires $\varepsilon_a = \varepsilon_{i-a}$ and $\varepsilon_s = \varepsilon_{i-s}$, which leads to the following coupled singular integral equations in dimensionless form

$$\lambda_a \int_{-1}^{X_a} T_a(\Xi_a)\,d\Xi_a + \int_{-1}^{1} \frac{T_a(\Xi_a)}{X_a - \Xi_a} d\Xi_a + \int_{-1}^{1} T_a(\Xi_a)\,d\Xi_a \int_0^{+\infty} f\left(\frac{\Theta}{a}\right) \sin[(X_a - \Xi_a)\Theta]\,d\Theta$$
$$+ \frac{K_a}{K_s} \int_{-1}^{1} \frac{T_s(\Xi_s)}{[(aX_a - l)/b] - \Xi_s} d\Xi_s + \frac{K_a}{K_s} \int_{-1}^{1} T_s(\Xi_s)\,d\Xi_s \int_0^{+\infty} f\left(\frac{\Theta}{b}\right)$$
$$\times \sin\left[\left(\frac{aX_a - l}{b} - \Xi_s\right)\Theta\right] d\Theta = 1 \quad (-1 < X_a < 1), \tag{3.22}$$

and

$$\lambda_s \int_{-1}^{X_s} T_s(\Xi_s)\,d\Xi_s + \int_{-1}^{1} \frac{T_s(\Xi_s)}{X_s - \Xi_s} d\Xi_s + \int_{-1}^{1} T_s(\Xi_s)\,d\Xi_s \int_0^{+\infty} f\left(\frac{\Theta}{b}\right) \sin[(X_s - \Xi_s)\Theta]\,d\Theta$$
$$+ \frac{K_s}{K_a} \int_{-1}^{1} \frac{T_a(\Xi_a)}{[(bX_s + l)/a] - \Xi_a} d\Xi_a + \frac{K_s}{K_a} \int_{-1}^{1} T_a(\Xi_a)\,d\Xi_a \int_0^{+\infty} f\left(\frac{\Theta}{a}\right)$$
$$\times \sin\left[\left(\frac{bX_s + l}{a} - \Xi_a\right)\Theta\right] d\Theta = 0 \quad (-1 < X_s < 1) \tag{3.23}$$

where $X_a = x_a/a$, $X_s = x_s/b$, function f is given by equation (3.12), and the other involved dimensionless functions and parameters are defined as

$$T_a(\Xi_a) = \frac{1}{\lambda_a} \frac{a}{h_{PZT}} \frac{\tau_a(a\Xi_a)}{e_p E_z} \quad \text{and} \quad T_s(\Xi_s) = \frac{1}{\lambda_s} \frac{b}{h_{PZT}} \frac{\tau_s(b\Xi_s)}{e_p E_z}, \tag{3.24}$$

and

$$\lambda_a = \frac{2\pi a(E_{encap} + E_{epidermis})}{3K_a} \quad \text{and} \quad \lambda_s = \frac{2\pi b(E_{encap} + E_{epidermis})}{3K_s}. \tag{3.25}$$

The solution of the coupled singular integral equations (3.22) and (3.23) has a square-root singularity at $\Xi = \pm 1$. Therefore, the shear force can be generally expressed in terms of the expansion of Chebyshev polynomials of the first kind as follows [26]

$$T_a(\Xi_a) = \frac{1}{\sqrt{1 - \Xi_a^2}} \sum_{n=1}^{+\infty} C_n^a T_n(\Xi_a) \quad \text{and} \quad T_s(\Xi_s) = \frac{1}{\sqrt{1 - \Xi_s^2}} \sum_{n=1}^{+\infty} C_n^s T_n(\Xi_s), \tag{3.26}$$

where T_n is the nth-order Chebyshev polynomial of the first kind, and C_n^a and C_n^s are the coefficients to be determined. Equation (3.26) satisfies the force equilibrium conditions in equation (3.1) and also the boundary conditions for the axial force at two ends of the actuator or the sensor as follows

$$\sum_{k=1}^{7} \sigma_a^{(k)}(\pm a) h^{(k)} = 0 \quad \text{and} \quad \sum_{k=1}^{7} \sigma_s^{(k)}(\pm b) h^{(k)} = 0, \tag{3.27}$$

owing to the orthogonality of Chebyshev polynomials.

Substitution of equation (3.26) into equations (3.22) and (3.23) leads to a set of linear algebraic equations for determining the coefficients C_n^a and C_n^s (see appendix C for details). Their dependence on the Young moduli $E_{epidermis}$ and E_{dermis} of the epidermis and dermis and the thickness $H_{epidermis}$ of epidermis is through three dimensionless parameters: $H_{epidermis}/a$, $\alpha_{epidermis}^{encap}$ and $\alpha_{dermis}^{epidermis}$. The ratio of the output voltage of the sensor to the input voltage of the actuator is related to the coefficient C_1^s by

$$\frac{U_{output}}{U_{input}} = -\frac{\pi^2}{6} \frac{e_p^2 h_{PZT}/k_e}{K_s} \frac{(E_{encap} + E_{epidermis})b}{K_s} C_1^s. \tag{3.28}$$

Downloaded from http://rspa.royalsocietypublishing.org/ on December 5, 2016

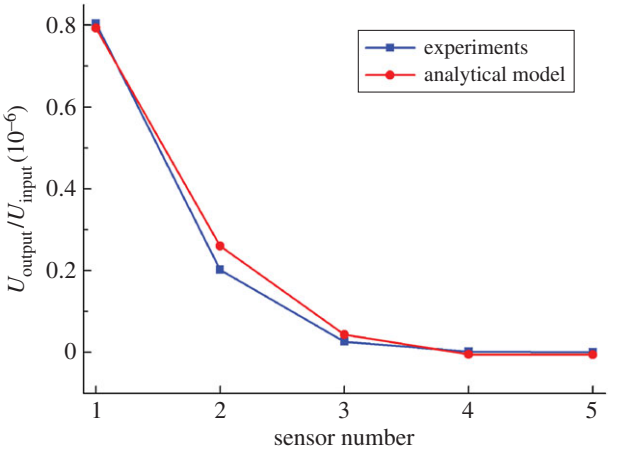

Figure 2. The output voltage of several sensors, normalized by the input voltage of the actuator, is obtained from the analytic model and experiments. (Online version in colour.)

(d) Comparison with experiments

The above-mentioned analytical model is validated by comparing with a model experiment with a 150 µm thick, relatively stiff poly(dimethylsiloxane) (PDMS, Young's modulus 1800 kPa) on a thick soft PDMS (Young's modulus 10 kPa). Their large mismatch in Young's moduli gives $\alpha_{\text{dermis}}^{\text{epidermis}} \approx 1$ from equation (3.17). The CMS system, mounted on the surface of the stiff PDMS, has a silicone encapsulation layer with the Young modulus $E_{\text{encap}} = 60$ kPa and thickness $H_{\text{encap}} = 20$ µm. The large elastic mismatch between the encapsulation layer and stiff PDMS gives $\alpha_{\text{epidermis}}^{\text{encap}} \approx 1$. The CMS system consists of one actuator (length $2a = 140$ µm) and five identical sensors (length $2b = 60$ µm), with the distance between the centres of the actuator and the sensors l = 300, 900, 1500, 2100 and 2700 µm, respectively. The detailed structures of the actuator and sensors as well as their geometric and material parameters are given in appendix A. Figure 2 shows the output voltage of all five sensors, normalized by the input voltage of the actuator. The comparison indicates a good agreement between the data from our validation experiment and the prediction from our analytical model without any parameter fitting. For applications to the human skin, the comparison of experiments with the theory gives the real skin modulus.

The usefulness of the analytic model is to determine the Young modulus and thickness of the relatively stiff PDMS layer from the output voltage in the experiments by solving an inverse problem. For a CMS device with encapsulation (with known material and geometric parameters), the normalized output voltage in equation (3.28) depends on the Young modulus and thickness of the stiff PDMS layer. Minimization of the difference in the output voltage between the analytical model and experiments for all sensors gives the Young modulus 1600 kPa and thickness 140 µm, which are 11% and 6.7% less than their values in experiments. This error mainly results from two orders of magnitude in elastic mismatch between the stiff PDMS layer (1800 kPa) and the encapsulation layer (60 kPa) and the soft PDMS (10 kPa). It is expected that this error will decrease significantly for measurement of skin modulus, because the Young moduli of epidermis (approx. 10^2 kPa [24,32]), dermis (approx. 10^1 kPa [32]) and encapsulation layer (60 kPa) are all on the same order of magnitude.

4. A strategy to determine Young's moduli of epidermis and dermis

A strategy to simultaneously determine the Young moduli $E_{\text{epidermis}}$ and E_{dermis} and the thickness $H_{\text{epidermis}}$ is proposed in this section. Figures 3–5 show the output voltage of the sensor (length

Downloaded from http://rspa.royalsocietypublishing.org/ on December 5, 2016

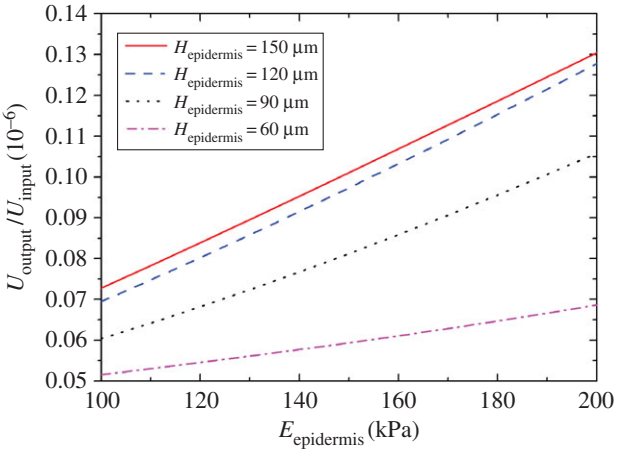

Figure 3. The normalized output voltage of the sensor versus the Young modulus of epidermis for several values of epidermis thickness. Here, $E_{dermis} = 30$ kPa. (Online version in colour.)

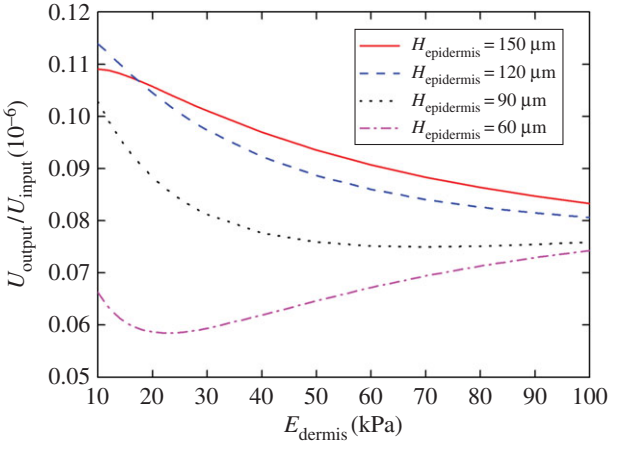

Figure 4. The normalized output voltage of the sensor versus the Young modulus of dermis for several values of epidermis thickness. Here, $E_{epidermis} = 150$ kPa. (Online version in colour.)

$2b = 60$ μm) on the Young moduli $E_{epidermis}$ of the epidermis and E_{dermis} of the dermis, and the thickness $H_{epidermis}$ of the epidermis layer, for the actuator length $2a = 140$ μm and a distance $l = 300$ μm between the actuator and sensor. The encapsulation layer has Young's modulus $E_{encap} = 60$ kPa and thickness $H_{encap} = 20$ μm. The output voltage of the sensor, normalized by the input voltage of the actuator, displays an approximately linear dependence on $E_{epidermis}$ (figure 3). However, its dependence on E_{dermis} and $H_{epidermis}$ are non-monotonic (figures 4 and 5). These non-monotonic dependences may create difficulties to uniquely determine E_{dermis} and $H_{epidermis}$, which is common for all inverse problems.

The CMS system is redesigned in the following to scale its size proportionally as $(2a, 2b, l) = \lambda$ (140, 60, 300 μm), where λ is the scaling factor. For $E_{epidermis} = 150$ kPa, $E_{dermis} = 30$ kPa, $E_{encap} = 60$ kPa and thickness $H_{encap} = 20$ μm, figure 6 shows the normalized output voltage of the sensor versus the scaling factor λ for several values of $H_{epidermis}$ ranging from 50 to 200 μm. The output voltage of the sensor increases monotonically with λ either $\lambda \leq 1/5$ or $\lambda \geq 5$, which correspond to small and large sizes, respectively, when compared with the thickness of the epidermis. For $\lambda \leq 1/5$, the output voltage of the sensor is insensitive to the thickness of the epidermis, which suggests that the effects of both the thickness of the epidermis and the modulus

Downloaded from http://rspa.royalsocietypublishing.org/ on December 5, 2016

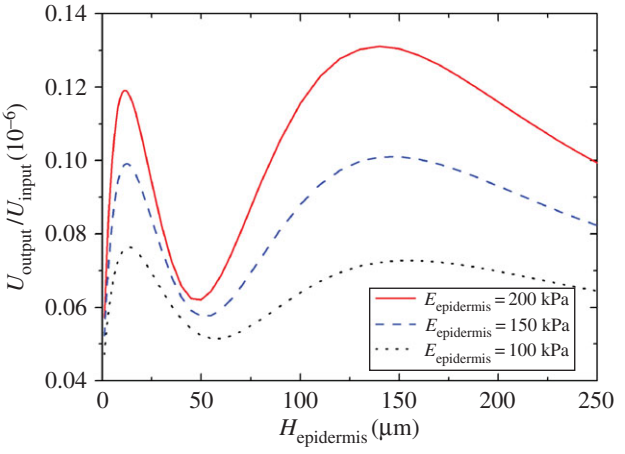

Figure 5. The normalized output voltage of the sensor versus the thickness of the epidermis for several values of epidermis modulus. Here, $E_{dermis} = 30$ kPa. (Online version in colour.)

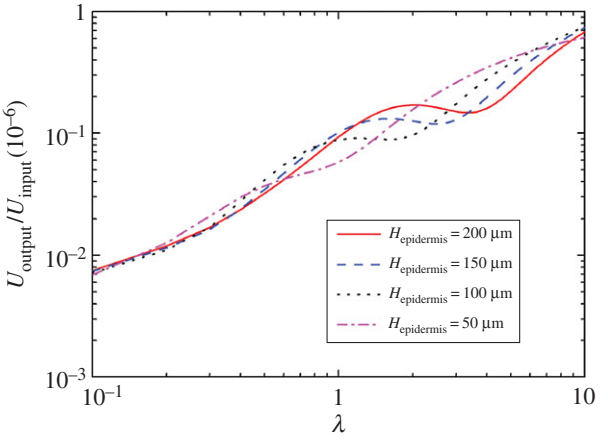

Figure 6. The normalized output voltage of the sensor versus the scaling factor λ for several values of epidermis thickness. Here, $E_{epidermis} = 150$ kPa and $E_{dermis} = 30$ kPa. (Online version in colour.)

of dermis are negligible. These observations suggest the use of a CMS system consisting of two sets of actuator/sensors. One set has small-size actuator and sensors with ($2a_{small}$, $2b_{small}$, l_{small}) approximately one-fifth of the representative thickness of the epidermis, to determine $E_{epidermis}$ independently. Another set has large-size actuator and sensors with ($2a_{large}$, $2b_{large}$, l_{large}) approximately five times of the thickness of the epidermis, to determine E_{dermis} and $H_{epidermis}$ simultaneously after $E_{epidermis}$ is determined.

5. Concluding remarks

An analytic model is developed for use of a CMS system to determine the Young moduli of the skin, including the epidermis and the dermis, as well as the thickness of the epidermis. The piezoelectric thin-film actuator and sensors in the CMS system interact with the human skin as well as the encapsulation layer through the interfacial shear stress distribution over the surface of the actuator and sensors. The analytical model agrees well with the *in vitro* experiments for a bilayer structure of PDMS, without any parameter fitting. For evaluation of human skin, the analytical model suggests a design for a CMS system that consists of two sets of actuator and

Downloaded from http://rspa.royalsocietypublishing.org/ on December 5, 2016

sensors. A set of small-size actuator and sensors determines the Young modulus of epidermis, whereas a set of large-size actuator and sensors determine the thickness of the epidermis and the Young modulus of dermis.

Ethics. The research work did not involve active collection of human data or any other ethical issues.

Data accessibility. The datasets supporting this article are already available in the article itself.

Author's contributions. J.Y. carried out the analytic modelling, analysed the data and drafted the manuscript; C.D. carried out the experiments, participated in data analysis and revised the manuscript; Y.S. participated in the analytical modelling and discussions; Y.M. participated in data analysis and discussions; X.F. and J.A.R. analysed the data and revised the manuscript; Y.H. designed the study, analysed the data and finalized the manuscript. All authors gave final approval for publication.

Competing interests. The authors declare that they have no competing interests.

Funding. J.Y. acknowledges the support from the National Natural Science Foundation of China (grant no. 11402133). X.F. acknowledges the support from the National Basic Research Programme of China (grant no. 2015CB351900) and the National Natural Science Foundation of China (grant no. 11320101001). Y.H. acknowledges the support from the US National Science Foundation (grant nos. DMR-1121262, CMMI-1534120, CMMI-1300846 and CMMI-1400169) and from the US National Institutes of Health (grant no. R01EB019337).

Acknowledgements. The authors thank the reviewers for their helpful comments and suggestions.

Appendix A

The actuator or sensor in the CMS system [24] consist of seven layers

$$\left.\begin{aligned}
&\text{PI } (h_1 = 2.4\mu\text{m}, E_1 = 2.5\,\text{GPa}, \nu_1 = 0.34)\\
&\text{Au } (h_2 = 300\,\text{nm}, E_2 = 78\,\text{GPa}, \nu_2 = 0.44)\\
&\text{Cr } (h_3 = 10\,\text{nm}, E_3 = 279\,\text{GPa}, \nu_3 = 0.21)\\
&\text{PZT } (h_4 = 500\,\text{nm})\\
&\text{Pt } (h_5 = 300\,\text{nm}, E_5 = 168\,\text{GPa}, \nu_5 = 0.38)\\
&\text{Ti } (h_6 = 20\text{nm}, E_6 = 110\,\text{GPa}, \nu_6 = 0.34)\\
\text{and}\quad &\text{PI } (h_7 = 1.2\mu\text{m}, E_7 = 2.5\text{GPa}, \nu_7 = 0.34),
\end{aligned}\right\} \tag{A 1}$$

where h_k, E_k and ν_k denote the thickness, Young's modulus and Poisson's ratio of the kth elastic layer, respectively. The polyimide (PI) layer on the Au-electrode side is in direct contact with the skin.

The PZT layer (layer 4) in the actuator or sensor is transversely isotropic with its poling direction along the layer thickness. Their elastic, piezoelectric and dielectric coefficients are [33]

$$\left.\begin{aligned}
&c_{11} = 139\,\text{GPa}, \quad c_{12} = 77.8\,\text{GPa}, \quad c_{13} = 74.3\,\text{GPa},\\
&c_{33} = 113\,\text{GPa}, \quad c_{44} = 25.6\,\text{GPa}, \quad c_{66} = \frac{(c_{11} - c_{12})}{2};\\
&e_{31} = -6.98\,\text{C m}^{-2}, \quad e_{33} = 13.8\,\text{C m}^{-2}, \quad e_{15} = 13.4\,\text{C m}^{-2}\\
\text{and}\quad &k_{11} = 6.0 \times 10^{-9}\,\text{C}^2\,(\text{Nm}^2)^{-1}, \quad k_{33} = 5.47 \times 10^{-9}\,\text{C}^2\,(\text{Nm}^2)^{-1}.
\end{aligned}\right\} \tag{A 2}$$

Appendix B

The fundamental solution for the layered half-plane owing to a horizontal unit point-force at the interface is obtained below, following the method of reverberation ray matrix [28–30]. The

Downloaded from http://rspa.royalsocietypublishing.org/ on December 5, 2016

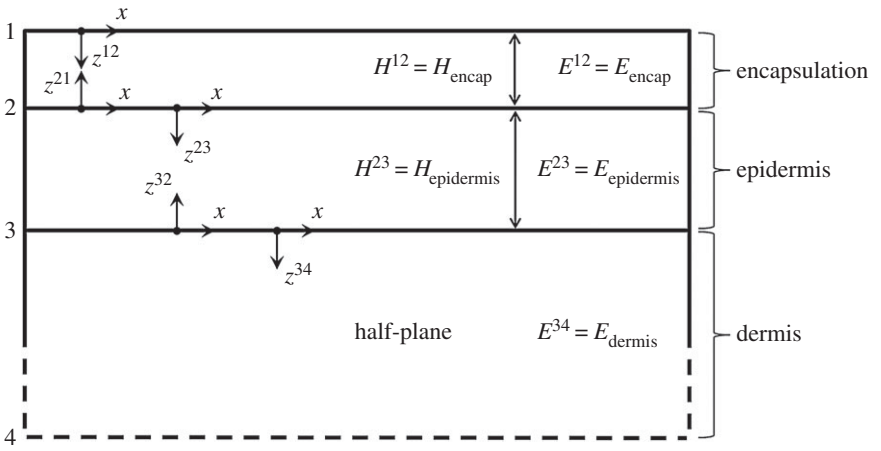

Figure 7. Dual coordinates for the encapsulation, epidermis and dermis.

general solution for the displacements and stresses in an incompressible medium under plane-strain condition can be expressed as

$$\left.\begin{aligned} u_1 &= \frac{\partial \varphi_1}{\partial x} + z\frac{\partial \varphi_2}{\partial x}, \quad u_3 = \frac{\partial \varphi_1}{\partial z} + z\frac{\partial \varphi_2}{\partial z} - \varphi_2 \\ \text{and} \qquad \sigma_{31} &= \frac{2E}{3}\left(\frac{\partial^2 \varphi_1}{\partial x \partial z} + z\frac{\partial^2 \varphi_2}{\partial x \partial z}\right), \quad \sigma_{33} = \frac{2E}{3}\left(\frac{\partial^2 \varphi_1}{\partial z^2} + z\frac{\partial^2 \varphi_2}{\partial z^2} - \frac{\partial \varphi_2}{\partial z}\right) \end{aligned}\right\}, \tag{B 1}$$

where E is Young's modulus, and φ_1 and φ_2 are two harmonic functions that satisfy

$$\frac{\partial^2 \varphi_1}{\partial x^2} + \frac{\partial^2 \varphi_1}{\partial z^2} = 0 \quad \text{and} \quad \frac{\partial^2 \varphi_2}{\partial x^2} + \frac{\partial^2 \varphi_2}{\partial z^2} = 0. \tag{B 2}$$

The application of the Fourier transform

$$\hat{f}(k) = \int_{-\infty}^{+\infty} f(x)\, \mathrm{e}^{-\mathrm{i}kx}\, \mathrm{d}x, \tag{B 3}$$

to equations (B 1) and (B 2) gives the general solutions of displacements and stresses in the transformed domain as

$$\left.\begin{aligned} \hat{u}_1(z; A_\xi, D_\xi) &= \mathrm{i}k[(A_1\, \mathrm{e}^{|k|z} + D_1\, \mathrm{e}^{-|k|z}) + z(A_2\, \mathrm{e}^{|k|z} + D_2\, \mathrm{e}^{-|k|z})] \\ \hat{u}_3(z; A_\xi, D_\xi) &= |k|(A_1\, \mathrm{e}^{|k|z} - D_1\, \mathrm{e}^{-|k|z}) - (A_2\, \mathrm{e}^{|k|z} + D_2\, \mathrm{e}^{-|k|z}) \\ &\quad + |k|z(A_2\, \mathrm{e}^{|k|z} - D_2\, \mathrm{e}^{-|k|z}) \\ \hat{\sigma}_{31}(z; A_\xi, D_\xi) &= \frac{2E}{3}\mathrm{i}k|k|[(A_1\, \mathrm{e}^{|k|z} - D_1\, \mathrm{e}^{-|k|z}) + z(A_2\, \mathrm{e}^{|k|z} - D_2\, e^{-|k|z})] \\ \hat{\sigma}_{33}(z; A_\xi, D_\xi) &= \frac{2E}{3}[k^2(A_1\, \mathrm{e}^{|k|z} + D_1\, \mathrm{e}^{-|k|z}) + k^2 z(A_2\, \mathrm{e}^{|k|z} + D_2\, \mathrm{e}^{-|k|z}) \\ &\quad - |k|(A_2\, \mathrm{e}^{|k|z} - D_2\, \mathrm{e}^{-|k|z})] \end{aligned}\right\} \quad \text{for } \xi = 1, 2, \tag{B 4}$$

where $|k|$ denotes the absolute value of k, and $A_\xi = 0$ for the semi-infinite medium shown in figure 7, which also shows dual local coordinate systems, distinguished by the superscripts, for each layer. For convenience, we label the modulus (and thickness) of the encapsulation layer, epidermis and dermis by the superscripts 12, 23 and 34, respectively. The general solutions for

Downloaded from http://rspa.royalsocietypublishing.org/ on December 5, 2016

the encapsulation layer and epidermis in dual local coordinates can be expressed as

$$\left.\begin{array}{ll} \hat{u}_1(z^{IJ};A_\xi^{IJ},D_\xi^{IJ}) & \hat{u}_1(z^{JI};A_\xi^{JI},D_\xi^{JI}) \\ \hat{u}_3(z^{IJ};A_\xi^{IJ},D_\xi^{IJ}) & \hat{u}_3(z^{JI};A_\xi^{JI},D_\xi^{JI}) \\ \hat{\sigma}_{31}(z^{IJ};A_\xi^{IJ},D_\xi^{IJ}) & \hat{\sigma}_{31}(z^{JI};A_\xi^{JI},D_\xi^{JI}) \\ \hat{\sigma}_{33}(z^{IJ};A_\xi^{IJ},D_\xi^{IJ}) & \hat{\sigma}_{33}(z^{JI};A_\xi^{JI},D_\xi^{JI}) \end{array}\right\} \quad \text{or} \quad \text{for } IJ=12,23, \tag{B 5}$$

and that for dermis in local coordinates as

$$\hat{u}_1(z^{34};0,D_\xi^{34}),\quad \hat{u}_3(z^{34};0,D_\xi^{34}),\quad \hat{\sigma}_{31}(z^{34};0,D_\xi^{34}) \quad \text{and} \quad \hat{\sigma}_{33}(z^{34};0,D_\xi^{34}). \tag{B 6}$$

The two sets of solutions in equation (B 5) should satisfy the following relations

$$\left.\begin{aligned} \hat{u}_1(z^{IJ};A_\xi^{IJ},D_\xi^{IJ}) &= \hat{u}_1(H^{IJ}-z^{IJ};A_\xi^{JI},D_\xi^{JI}) \\ \hat{u}_3(z^{IJ};A_\xi^{IJ},D_\xi^{IJ}) + \hat{u}_3(H^{IJ}-z^{IJ};A_\xi^{JI},D_\xi^{JI}) &= 0 \\ \hat{\sigma}_{31}(z^{IJ};A_\xi^{IJ},D_\xi^{IJ}) + \hat{\sigma}_{31}(H^{IJ}-z^{IJ};A_\xi^{JI},D_\xi^{JI}) &= 0 \\ \hat{\sigma}_{33}(z^{IJ};A_\xi^{IJ},D_\xi^{IJ}) &= \hat{\sigma}_{33}(H^{IJ}-z^{IJ};A_\xi^{JI},D_\xi^{JI}) \end{aligned}\right\} \quad \text{for } IJ=12,23, \tag{B 7}$$

which leads to

$$\begin{Bmatrix} A_1^{IJ} \\ A_2^{IJ} \\ A_1^{JI} \\ A_2^{JI} \end{Bmatrix} = \mathbf{P}(H^{IJ}) \begin{Bmatrix} D_1^{IJ} \\ D_2^{IJ} \\ D_1^{JI} \\ D_2^{JI} \end{Bmatrix} \quad \text{for } IJ=12,23, \tag{B 8}$$

with

$$\mathbf{P}(H^{IJ}) = \begin{bmatrix} 0 & 0 & \mathrm{e}^{-|k|H^{IJ}} & H^{IJ}\,\mathrm{e}^{-|k|H^{IJ}} \\ 0 & 0 & 0 & -\mathrm{e}^{-|k|H^{IJ}} \\ \mathrm{e}^{-|k|H^{IJ}} & H^{IJ}\,\mathrm{e}^{-|k|H^{IJ}} & 0 & 0 \\ 0 & -\mathrm{e}^{-|k|H^{IJ}} & 0 & 0 \end{bmatrix}. \tag{B 9}$$

The traction-free surface of encapsulation layer and the perfectly bonded interfaces between adjacent layers require

$$\left.\begin{aligned} \hat{\sigma}_{31}(0;A_\xi^{12},D_\xi^{12}) &= 0 \\ \text{and} \quad \hat{\sigma}_{33}(0;A_\xi^{12},D_\xi^{12}) &= 0, \end{aligned}\right\} \tag{B 10}$$

$$\left.\begin{aligned} \hat{u}_1(0;A_\xi^{23},D_\xi^{23}) &= \hat{u}_1(0;A_\xi^{21},D_\xi^{21}) \\ \hat{u}_3(0;A_\xi^{23},D_\xi^{23}) + \hat{u}_3(0;A_\xi^{21},D_\xi^{21}) &= 0 \\ \hat{\sigma}_{31}(0;A_\xi^{23},D_\xi^{23}) + \hat{\sigma}_{31}(0;A_\xi^{21},D_\xi^{21}) + 1 &= 0 \\ \text{and} \quad \hat{\sigma}_{33}(0;A_\xi^{23},D_\xi^{23}) &= \hat{\sigma}_{33}(0;A_\xi^{21},D_\xi^{21}), \end{aligned}\right\} \tag{B 11}$$

and

$$\left.\begin{aligned} \hat{u}_1(0;0,D_\xi^{34}) &= \hat{u}_1(0;A_\xi^{32},D_\xi^{32}) \\ \hat{u}_3(0;0,D_\xi^{34}) + \hat{u}_3(0;A_\xi^{32},D_\xi^{32}) &= 0 \\ \hat{\sigma}_{31}(0;0,D_\xi^{34}) + \hat{\sigma}_{31}(0;A_\xi^{32},D_\xi^{32}) + 1 &= 0 \\ \text{and} \quad \hat{\sigma}_{33}(0;0,D_\xi^{34}) &= \hat{\sigma}_{33}(0;A_\xi^{32},D_\xi^{32}). \end{aligned}\right\} \tag{B 12}$$

Downloaded from http://rspa.royalsocietypublishing.org/ on December 5, 2016

Equations (B 10), (B 11) and (B 12) can be rewritten as

$$\mathbf{S}_1 \begin{Bmatrix} A_1^{12} \\ A_2^{12} \end{Bmatrix} + \begin{Bmatrix} D_1^{12} \\ D_2^{12} \end{Bmatrix} = 0, \tag{B 13}$$

$$\mathbf{S}_2 \begin{Bmatrix} A_1^{21} \\ A_2^{21} \\ A_1^{23} \\ A_2^{23} \end{Bmatrix} + \begin{Bmatrix} D_1^{21} \\ D_2^{21} \\ D_1^{23} \\ D_2^{23} \end{Bmatrix} = \frac{3}{E^{12}+E^{23}} \frac{1}{2\mathrm{i}k|k|} \begin{Bmatrix} 1 \\ -|k| \\ 1 \\ -|k| \end{Bmatrix} \tag{B 14}$$

and

$$\mathbf{S}_3 \begin{Bmatrix} A_1^{32} \\ A_2^{32} \end{Bmatrix} + \begin{Bmatrix} D_1^{32} \\ D_2^{32} \\ D_1^{34} \\ D_2^{34} \end{Bmatrix} = 0, \tag{B 15}$$

where

$$\mathbf{S}_1 = \begin{bmatrix} -1 & 0 \\ 2|k| & -1 \end{bmatrix}, \tag{B 16}$$

$$\mathbf{S}_2 = \begin{bmatrix} -\alpha_2 & 0 & -1+\alpha_2 & 0 \\ 2\alpha_2|k| & -\alpha_2 & 0 & 1-\alpha_2 \\ -1-\alpha_2 & 0 & \alpha_2 & 0 \\ 0 & 1+\alpha_2 & -2\alpha_2|k| & \alpha_2 \end{bmatrix} \tag{B 17}$$

and

$$\mathbf{S}_3 = \begin{bmatrix} -\alpha_3 & 0 \\ 2\alpha_3|k| & -\alpha_3 \\ -1-\alpha_3 & 0 \\ 0 & 1+\alpha_3 \end{bmatrix}, \tag{B 18}$$

with

$$\alpha_2 = \frac{E^{12}-E^{23}}{E^{12}+E^{23}} \quad \text{and} \quad \alpha_3 = \frac{E^{23}-E^{34}}{E^{23}+E^{34}}. \tag{B 19}$$

Equations (B 13), (B 14) and (B 15), together with equation (B 8), yield

$$\left.\begin{aligned} \mathbf{D}_{10\times1} &= \frac{3}{E^{12}+E^{23}} \frac{1}{2\mathrm{i}k|k|} (\mathbf{I}_{10\times10} + \mathbf{S}_{10\times8}\mathbf{P}_{8\times10})^{-1}\mathbf{s}_{10\times1} \\ \text{and} \quad \mathbf{A}_{8\times1} &= \mathbf{P}_{8\times10}\mathbf{D}_{10\times1} \end{aligned}\right\}, \tag{B 20}$$

where $\mathbf{I}_{10\times10}$ is the identity matrix

$$\left.\begin{aligned} \mathbf{D}_{10\times1} &= \{D_1^{12} \quad D_2^{12} \quad D_1^{21} \quad D_2^{21} \quad D_1^{23} \quad D_2^{23} \quad D_1^{32} \quad D_2^{32} \quad D_1^{34} \quad D_2^{34}\}^{\mathrm{T}} \\ \text{and} \quad \mathbf{A}_{8\times1} &= \{A_1^{12} \quad A_2^{12} \quad A_1^{21} \quad A_2^{21} \quad A_1^{23} \quad A_2^{23} \quad A_1^{32} \quad A_2^{32}\}^{\mathrm{T}} \end{aligned}\right\}, \tag{B 21}$$

$\mathbf{P}_{8\times10}$ and $\mathbf{S}_{10\times8}$ are the phase matrix and scattering matrix given by

$$\mathbf{P}_{8\times10} = \begin{bmatrix} \mathbf{P}(H^{12}) & \mathbf{0}_{4\times4} & \mathbf{0}_{4\times2} \\ \mathbf{0}_{4\times4} & \mathbf{P}(H^{23}) & \mathbf{0}_{4\times2} \end{bmatrix} \tag{B 22}$$

and

$$\mathbf{S}_{10\times8} = \begin{bmatrix} \mathbf{S}_1 & \mathbf{0}_{2\times4} & \mathbf{0}_{2\times2} \\ \mathbf{0}_{4\times2} & \mathbf{S}_2 & \mathbf{0}_{4\times2} \\ \mathbf{0}_{4\times2} & \mathbf{0}_{4\times4} & \mathbf{S}_3 \end{bmatrix}, \tag{B 23}$$

Downloaded from http://rspa.royalsocietypublishing.org/ on December 5, 2016

respectively, and $\mathbf{s}_{10\times1}$ is the source vector

$$\mathbf{s}_{10\times1}=\{0\quad 0\quad 1\quad -|k|\quad 1\quad -|k|\quad 0\quad 0\quad 0\quad 0\}^{\mathrm{T}}. \tag{B 24}$$

By the inverse Fourier transform

$$f(x)=\frac{1}{2\pi}\int_{-\infty}^{+\infty}\hat{f}(k)\,\mathrm{e}^{\mathrm{i}kx}\,\mathrm{d}k, \tag{B 25}$$

the normal strain in the x-direction along the encapsulation/epidermis interface can be derived in the physical domain from equations (B 4), (B 8) and (B 20) as

$$\begin{aligned}\varepsilon_{11}(x)&=\frac{\partial}{\partial x}\left[\frac{1}{2\pi}\int_{-\infty}^{+\infty}\hat{u}_1(0;A_\xi^{21},D_\xi^{21})\,\mathrm{e}^{\mathrm{i}kx}\,\mathrm{d}k\right]\\&=-\frac{1}{4\pi\mathrm{i}}\frac{3}{E^{12}+E^{23}}\int_{-\infty}^{+\infty}\frac{k}{|k|}\{\mathrm{e}^{-|k|H^{12}}\quad H^{12}\,\mathrm{e}^{-|k|H^{12}}\quad 1\quad \mathbf{0}_{1\times7}\}(\mathbf{I}_{10\times10}+\mathbf{S}_{10\times8}\mathbf{P}_{8\times10})^{-1}\mathbf{s}_{10\times1}\,\mathrm{e}^{\mathrm{i}kx}\,\mathrm{d}k\\&=-\frac{1}{2\pi\mathrm{i}}\frac{3}{E^{12}+E^{23}}\int_{0}^{+\infty}\{\mathrm{e}^{-kH^{12}}\quad H^{12}\,\mathrm{e}^{-kH^{12}}\quad 1\quad \mathbf{0}_{1\times7}\}(\mathbf{I}_{10\times10}+\mathbf{S}_{10\times8}\mathbf{P}_{8\times10})^{-1}\mathbf{s}_{10\times1}\sin(kx)\,\mathrm{d}k,\end{aligned} \tag{B 26}$$

Equation (B 26) can be further decomposed into two separate parts as

$$\varepsilon_{11}(x)=\varepsilon_{11}^{\text{bi-material}}(x)+\varepsilon_{11}^{\mathrm{c}}(x), \tag{B 27}$$

where $\varepsilon_{11}^{\text{bi-material}}$ denotes the normal strain in the x-direction along the encapsulation/epidermis interface owing to the same force in the corresponding bi-material composed of an encapsulation half-plane and an epidermis half-plane defined as

$$\begin{aligned}\varepsilon_{11}^{\text{bi-material}}(x)&=-\frac{1}{4\pi\mathrm{i}}\frac{3}{E^{12}+E^{23}}\int_{-\infty}^{+\infty}\frac{k}{|k|}\{\mathrm{e}^{-|k|H^{12}}\quad H^{12}\,\mathrm{e}^{-|k|H^{12}}\quad 1\quad \mathbf{0}_{1\times7}\}\mathbf{s}_{10\times1}\,\mathrm{e}^{\mathrm{i}kx}\,\mathrm{d}k\\&=-\frac{1}{4\pi\mathrm{i}}\frac{3}{E^{12}+E^{23}}\int_{-\infty}^{+\infty}\frac{k}{|k|}\,\mathrm{e}^{\mathrm{i}kx}\,\mathrm{d}k=-\frac{3}{2\pi(E^{12}+E^{23})}\frac{1}{x},\end{aligned} \tag{B 28}$$

and $\varepsilon_{11}^{\mathrm{c}}$ is the complementary part defined as

$$\begin{aligned}\varepsilon_{11}^{\mathrm{c}}(x)&=-\frac{1}{4\pi\mathrm{i}}\frac{3}{E^{12}+E^{23}}\\&\quad\times\int_{-\infty}^{+\infty}\frac{k}{|k|}\{\mathrm{e}^{-|k|H^{12}}\quad H^{12}\,\mathrm{e}^{-|k|H^{12}}\quad 1\quad \mathbf{0}_{1\times7}\}[(\mathbf{I}_{10\times10}+\mathbf{S}_{10\times8}\mathbf{P}_{8\times10})^{-1}-\mathbf{I}_{10\times10}]\mathbf{s}_{10\times1}\,\mathrm{e}^{\mathrm{i}kx}\,\mathrm{d}k\\&=-\frac{1}{2\pi}\frac{3}{E^{12}+E^{23}}\\&\quad\times\int_{0}^{+\infty}\{\mathrm{e}^{-kH^{12}}\quad H^{12}\,\mathrm{e}^{-kH^{12}}\quad 1\quad \mathbf{0}_{1\times7}\}[(\mathbf{I}_{10\times10}+\mathbf{S}_{10\times8}\mathbf{P}_{8\times10})^{-1}-\mathbf{I}_{10\times10}]\mathbf{s}_{10\times1}\sin(kx)\,\mathrm{d}k.\end{aligned} \tag{B 29}$$

Appendix C

The infinite series in equation (3.26) for the normalized shear stress is truncated to the Nth term when substituted into equations (3.22) and (3.23). Multiplying $\sqrt{1-X_{\mathrm{a}}^2}U_{m-1}(X_{\mathrm{a}})$ and $\sqrt{1-X_{\mathrm{s}}^2}U_{m-1}(X_{\mathrm{s}})$ on both sides of equations (3.22) and (3.23), and then integration from -1 to $+1$ with respect to X_{a} and X_{s}, respectively, give a set of linear algebraic equations for C_n^{a} and C_n^{s}

Downloaded from http://rspa.royalsocietypublishing.org/ on December 5, 2016

as

$$\left.\begin{aligned}\sum_{n=1}^{N}(\Lambda_{mn}^{\mathrm{a-a}}C_n^{\mathrm{a}}+\Lambda_{mn}^{\mathrm{a-s}}C_n^{\mathrm{s}})&=-\frac{1}{\pi}\delta_{m1}\\ \text{and}\qquad \sum_{n=1}^{N}(\Lambda_{mn}^{\mathrm{s-a}}C_n^{\mathrm{a}}+\Lambda_{mn}^{\mathrm{s-s}}C_n^{\mathrm{s}})&=0,\end{aligned}\right\}\tag{C 1}$$

where U_n is the nth-order Chebyshev polynomial of the second kind, δ_{ij} is the Kronecker delta, and

$$\left.\begin{aligned}\Lambda_{mn}^{\mathrm{a-a}}&=\delta_{mn}-\lambda_{\mathrm{a}}g_{mn}+\cos\frac{(m-n)\pi}{2}\int_0^{+\infty}\frac{2m}{\Theta}J_m(\Theta)J_n(\Theta)f\left(\frac{\Theta}{a}\right)\mathrm{d}\Theta\\ \Lambda_{mn}^{\mathrm{a-s}}&=\frac{K_{\mathrm{a}}}{K_{\mathrm{s}}}\int_0^{+\infty}\frac{2mb}{a\Theta}J_m\left(\frac{a\Theta}{b}\right)J_n(\Theta)\left[f\left(\frac{\Theta}{b}\right)+1\right]\cos\left[\frac{(m-n)\pi}{2}-\frac{l\Theta}{b}\right]\mathrm{d}\Theta\\ \Lambda_{mn}^{\mathrm{s-s}}&=\delta_{mn}-\lambda_{\mathrm{s}}g_{mn}+\cos\frac{(m-n)\pi}{2}\int_0^{+\infty}\frac{2m}{\Theta}J_m(\Theta)J_n(\Theta)f\left(\frac{\Theta}{b}\right)\mathrm{d}\Theta\\ \text{and}\qquad \Lambda_{mn}^{\mathrm{s-a}}&=\frac{K_{\mathrm{s}}}{K_{\mathrm{a}}}\int_0^{+\infty}\frac{2ma}{b\Theta}J_m\left(\frac{b\Theta}{a}\right)J_n(\Theta)\left[f\left(\frac{\Theta}{a}\right)+1\right]\cos\left[\frac{(m-n)\pi}{2}+\frac{l\Theta}{a}\right]\mathrm{d}\Theta\end{aligned}\right\},\tag{C 2}$$

with J_n being the nth-order Bessel function of the first kind. The function g_{mn} in equation (C 2) is defined as

$$g_{mn}=\begin{cases}\dfrac{4m[(-1)^{m-n}+1]}{\pi^2[(m-n)^2-1][(m+n)^2-1]}, & \text{if } (m-n)^2\neq 1;\\ 0, & \text{if } (m-n)^2=1\end{cases}.\tag{C 3}$$

References

1. Geerligs M, van Breemen L, Peters G, Ackermans P, Baaijens F, Oomens C. 2011 *in vitro* indentation to determine the mechanical properties of epidermis. *J. Biomech.* **44**, 1176–1181. (doi:10.1016/j.jbiomech.2011.01.015)
2. Hendriks FM, Brokken D, Oomens CWJ, Bader DL, Baaijens FPT. 2006 The relative contributions of different skin layers to the mechanical behavior of human skin *in vivo* using suction experiments. *Med. Eng. Phys.* **28**, 259–266. (doi:10.1016/j.medengphy.2005.07.001)
3. Pailler-Mattei C, Bec S, Zahouani H. 2008 *in vivo* measurements of the elastic mechanical properties of human skin by indentation tests. *Med. Eng. Phys.* **30**, 599–606. (doi:10.1016/j.medengphy.2007.06.011)
4. Hendriks FM, Brokken D, van Eemeren JTWM, Oomens CWJ, Baaijens FPT, Horsten JBAM. 2003 A numerical-experimental method to characterize the non-linear mechanical behaviour of human skin. *Skin Res. Technol.* **9**, 274–283. (doi:10.1034/j.1600-0846.2003.00019.x)
5. Agache PG, Monneur C, Leveque JL, De Rigal J. 1980 Mechanical properties and Young's modulus of human skin *in vivo*. *Arch. Dermatol. Res.* **269**, 221–232. (doi:10.1007/BF00406415)
6. Gennisson JL, Baldeweck T, Tanter M, Catheline S, Fink M, Sandrin L, Cornillon C, Querleux B. 2004 Assessment of elastic parameters of human skin using dynamic elastography. *IEEE Trans. Ultrason. Ferroelectr. Freq. Control* **51**, 980–989. (doi:10.1109/TUFFC.2004.1324402)
7. Diridollou S, Patat F, Gens F, Vaillant L, Black D, Lagarde JM, Gall Y, Berson M. 2000 *in vivo* model of the mechanical properties of the human skin under suction. *Skin Res. Technol.* **6**, 214–221. (doi:10.1034/j.1600-0846.2000.006004214.x)
8. Jasaitiene D, Valiukeviciene S, Linkeviciute G, Raisutis R, Jasiuniene E, Kazys R. 2011 Principles of high-frequency ultrasonography for investigation of skin pathology. *J. Eur. Acad. Dermatol. Venereol.* **25**, 375–382. (doi:10.1111/j.1468-3083.2010.03837.x)
9. Sanders R. 1973 Torsional elasticity of human skin *in vivo*. *Pflug. Arch. Eur. J. Physiol.* **342**, 255–260. (doi:10.1007/BF00591373)
10. Sugihara T, Ohura T, Homma K, Igawa HH. 1991 The extensibility in human skin: variation according to age and site. *Br. J. Plast. Surg.* **44**, 418–422. (doi:10.1016/0007-1226(91)90199-T)
11. Wang Q, Hayward V. 2007 *in vivo* biomechanics of the fingerpad skin under local tangential traction. *J. Biomech.* **40**, 851–860. (doi:10.1016/j.jbiomech.2006.03.004)

Downloaded from http://rspa.royalsocietypublishing.org/ on December 5, 2016

12. Li CH, Guan GY, Reif R, Huang ZH, Wang RK. 2012 Determining elastic properties of skin by measuring surface waves from an impulse mechanical stimulus using phase-sensitive optical coherence tomography. *J. R. Soc. Interface* **9**, 831–841. (doi:10.1098/rsif.2011.0583)
13. Rogers JA, Someya T, Huang Y. 2010 Materials and mechanics for stretchable electronics. *Science* **327**, 1603–1607. (doi:10.1126/science.1182383)
14. Shi Y, Dagdeviren C, Rogers JA, Gao CF, Huang Y. 2015 An analytic model for skin modulus measurement via conformal piezoelectric systems. *J. Appl. Mech. Trans. ASME* **82**, 091007. (doi:10.1115/1.4030820)
15. Shi Y, Rogers JA, Gao CF, Huang Y. 2014 Multiple neutral axes in bending of a multiple-layer beam with extremely different elastic properties. *J. Appl. Mech. Trans. ASME* **81**, 114501. (doi:10.1115/1.4028465)
16. Shi X, Xu R, Li Y, Zhang Y, Ren Z, Gu J, Rogers JA, Huang Y. 2014 Mechanics design for stretchable, high areal coverage GaAs solar module on an ultrathin substrate. *J. Appl. Mech. Trans. ASME* **81**, 124502. (doi:10.1115/1.4028977)
17. Liu Z, Cheng H, Wu J. 2014 Mechanics of Solar Module on Structured Substrates. *J. Appl. Mech. Trans. ASME* **81**, 064502. (doi:10.1115/1.4026472)
18. Cheng HY, Wang SD. 2014 Mechanics of interfacial delamination in epidermal electronics systems. *J. Appl. Mech. Trans. ASME* **81**, 044501. (doi:10.1115/1.4025305)
19. Cheng H, Song J. 2014 A simply analytic study of buckled thin films on compliant substrates. *J. Appl. Mech. Trans. ASME* **81**, 024501. (doi:10.1115/1.4025306)
20. Wang Q, Zhao X. 2014 Phase diagrams of instabilities in compressed film-substrate systems. *J. Appl. Mech. Trans. ASME* **81**, 051004. (doi:10.1115/1.4025828)
21. Guo GD, Zhu Y. 2015 Cohesive-shear-lag modeling of interfacial stress transfer between a monolayer graphene and a polymer substrate. *J. Appl. Mech. Trans. ASME* **82**, 031005. (doi:10.1115/1.4029635)
22. Dagdeviren C *et al.* 2014 Conformable amplified lead zirconate titanate sensors with enhanced piezoelectric response for cutaneous pressure monitoring. *Nat. Commun.* **5**, 4496. (doi:10.1038/ncomms5496)
23. Dagdeviren C, Joe P, Tuzman OL, Park KI, Lee KJ, Shi Y, Huang Y, Rogers JA. In press. Recent progress in flexible and stretchable piezoelectric devices for mechanical energy harvesting, sensing and actuation. *Extr. Mech. Lett.* (doi:10.1016/j.eml.2016.05.015)
24. Dagdeviren C *et al.* 2015 Conformal piezoelectric systems for clinical and experimental characterization of soft tissue biomechanics. *Nat. Mater.* **14**, 728–736. (doi:10.1038/NMAT4289)
25. Zolfaghari A, Merefat M. 2011 A new predictive index for evaluating both thermal sensation and thermal response of the human body. *Build. Environ.* **46**, 855–862. (doi:10.1016/j.buildenv.2010.10.011)
26. Wang XD, Meguid SA. 2000 On the electroelastic behaviour of a thin piezoelectric actuator attached to an infinite host structure. *Int. J. Solids Struct.* **37**, 3231–3251. (doi:10.1016/S0020-7683(99)00118-3)
27. Wang XD, Huang GL. 2006 The coupled dynamic behavior of piezoelectric sensors bonded to elastic media. *J. Intell. Mater. Syst. Struct.* **17**, 883–894. (doi:10.1177/1045389X06061130)
28. Howard SM, Pao YH. 1998 Analysis and experiments on stress waves in planar trusses. *J. Eng. Mech. ASME* **124**, 884–891. (doi:10.1061/(ASCE)0733-9399(1998)124:8(884))
29. Pao YH, Su XY, Tian JY. 2000 Reverberation matrix method for propagation of sound in a multilayered liquid. *J. Sound Vib.* **230**, 743–760. (doi:10.1006/jsvi.1999.2675)
30. Su XY, Tian JY, Pao YH. 2002 Application of the reverberation-ray matrix to the propagation of elastic waves in a layered solid. *Int. J. Solids Struct.* **39**, 5447–5463. (doi:10.1016/S0020-7683(02)00358-X)
31. Dundurs J. 1969 Discussion: 'edge-bonded dissimilar orthogonal elastic wedges under normal and shear loading'. *J. Appl. Mech.* **36**, 650–652. (doi:10.1115/1.3564739)
32. Boonma A, Narayan RJ, Lee YS. 2013 Analytical modeling and evaluation of microneedles apparatus with deformable soft tissues for biomedical applications. *Comput. Aided Des. Appl.* **10**, 139–157. (doi:10.3722/cadaps.2013.139-157)
33. Fang DN, Liu JX. 2012 *Fracture mechanics of piezoelectric and ferroelectric solids* (*in Chinese*). Beijing, China: Tsinghua University Press.